Energy Storage Materials 63 (2023) 102981

Contents lists available at ScienceDirect

Energy Storage Materials

journal homepage: www.elsevier.com/locate/ensm

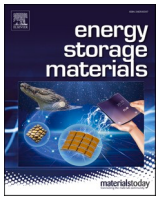

Dual-protected zinc anodes for long-life aqueous zinc ion battery with bifunctional interface constructed by zwitterionic surfactants

Li Tao [a,b,c,#,*], Kailin Guan [a,b,#], Rong Yang [a,b,#], Zhongxian Guo [a,b], Longyang Wang [a,b], Lei Xu [a,b], Houzhao Wan [a,b], Jun Zhang [a,b], Hanbin Wang [a,b], Linfeng Hu [d], Paul J. Dyson [c], Mohammad Khaja Nazeeruddin [c,*], Hao Wang [a,b,*]

[a] School of Microelectronics, Hubei University, Wuhan, 430062, PR China
[b] Hubei Yangtze Memory Laboratories, Wuhan, 430205, PR China
[c] Institute of Chemical Sciences and Engineering, Ecole Polytechnique Federale de Lausanne (EPFL), 1015, Lausanne, Switzerland
[d] School of Materials Science and Engineering, Southeast University Nanjing, 211189, PR China

ARTICLE INFO

Keywords:
Aqueous zinc ion battery
Zinc anode
Zinc dendrite
Zwitterionic surfactant
Dipole capping layer
Built-in electric field

ABSTRACT

The dendrite growth on the surface of zinc anodes and formation of inactive by-products of $Zn_4(OH)_6SO_4xH_2O$ (ZHS), mainly attributed to the "tip effect" of an uneven surface and water corrosion of zinc anode, have seriously shrunk the anode life and hindered the commercialization of aqueous zinc ion batteries (AZIBs). Herein, we describe a bifunctional interface constructed by zwitterionic surfactant of *N*-decyl-*N,N*-dimethyl-3-ammonio-1-propanesulfonate (Z10), which can form a polarized layer with a build-in electric field at the same time as the self-assembled hydrophobic layer on the zinc electrode surface. Two other zwitterionic surfactants including of *N*-octyl-*N,N*-dimethyl-3-ammonio-1-propanesulfonate (Z8) and *N*-tetradecyl-*N,N*-dimethyl-3-ammonio-1-propanesulfonate (Z14) are also selected, due to the different alkyl chain lengths affect the strength of the built-in electric field and the formation of hydrophobic interfaces. A combined results of experimental data with simulated calculations calculations confirm that the strength of the electric field obtained with Z10 attenuates the "tip effect" on the zinc anode surface, while accelerating the transfer of zinc ions and promoting rapid and uniform zinc plating/stripping processes. And benefited from the hydrophobic layer, the free water molecules are blocked outside the inner Helmholtz plane, lead to the suppressed ZHS formation. With the dual protection, in case of Z10, the cycle stability of the AZIBs is considerably improved to yield a long cycle lifetime of 2000 h with a coulombic efficiency of 99.4 %.

1. Introduction

With the rapid development of electric vehicles, portable electronic devices and grid-scale energy storage, there are increasing demands for efficient and safe energy storage devices with a long life and high energy density. Lithium-ion batteries (LIBs) are popular energy storage devices due to their high energy density and power density [1–3]. However, due to limited lithium reserves and insecurity, LIBs cannot be used for large energy storage with high stability and safety requirements [3–6]. In attempts to solve these issues, rapid progress in aqueous rechargeable batteries has been made in recent years. Among them, aqueous zinc ion batteries (AZIBs), owing to their high theoretical capacity (820 mAh g^{-1}), and low redox potential (−0.762 V vs SHE), are considered as one of the most promising candidates for batteries [7–11]. Unfortunately, at the zinc anode, water corrosion lead to side reactions and generation of inactive byproducts, such as $Zn_4(OH)_6SO_4xH_2O$ (ZHS), which prevents the efficient diffusion of zinc ions, passivating the zinc anode surface and reducing the utilization rate of zinc [12–14]. Moreover, the active sites with an uneven distributed electric field on the zinc anode surface have the priority for zinc ion electrodeposition during plating/stripping. As a result, the growth of zinc dendrites and "tip effect" are promoted [15]. Zinc dendrites with sharp, needle-like morphologies can pierce the separator and cause an electrical short circuit, shortening the cycle life and lowing the Coulombic efficiency (CE) of AZIBs. Therefore, inhibiting the formation of zinc dendrites and enhancing the stability are required if AZIBs are to be used for large-scale energy storage.

* Corresponding authors.
E-mail addresses: litao@hubu.edu.cn (L. Tao), mdkhaja.nazeeruddin@epfl.ch (M.K. Nazeeruddin), wangh@hubu.edu.cn (H. Wang).
Li Tao, Kailin Guan and Rong Yang contribute equally to this work.

https://doi.org/10.1016/j.ensm.2023.102981
Received 8 April 2023; Received in revised form 8 September 2023; Accepted 17 September 2023
Available online 23 September 2023

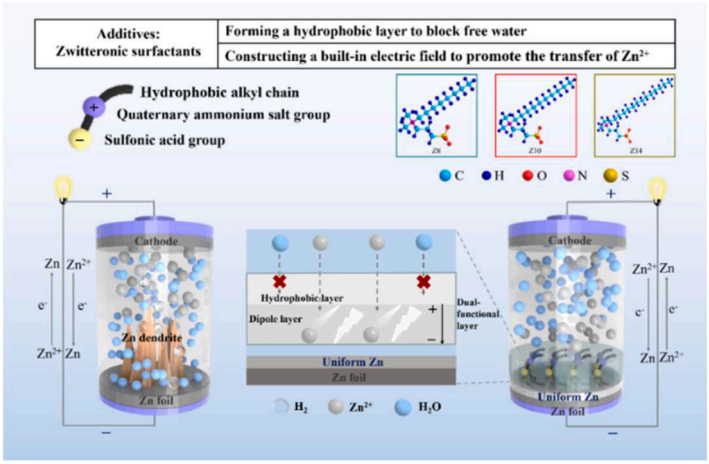

Fig. 1. Structures of the zwitterionic surfactants used as electrolyte additives and a schematic of the AZIBs without and with the zwitterionic surfactants.

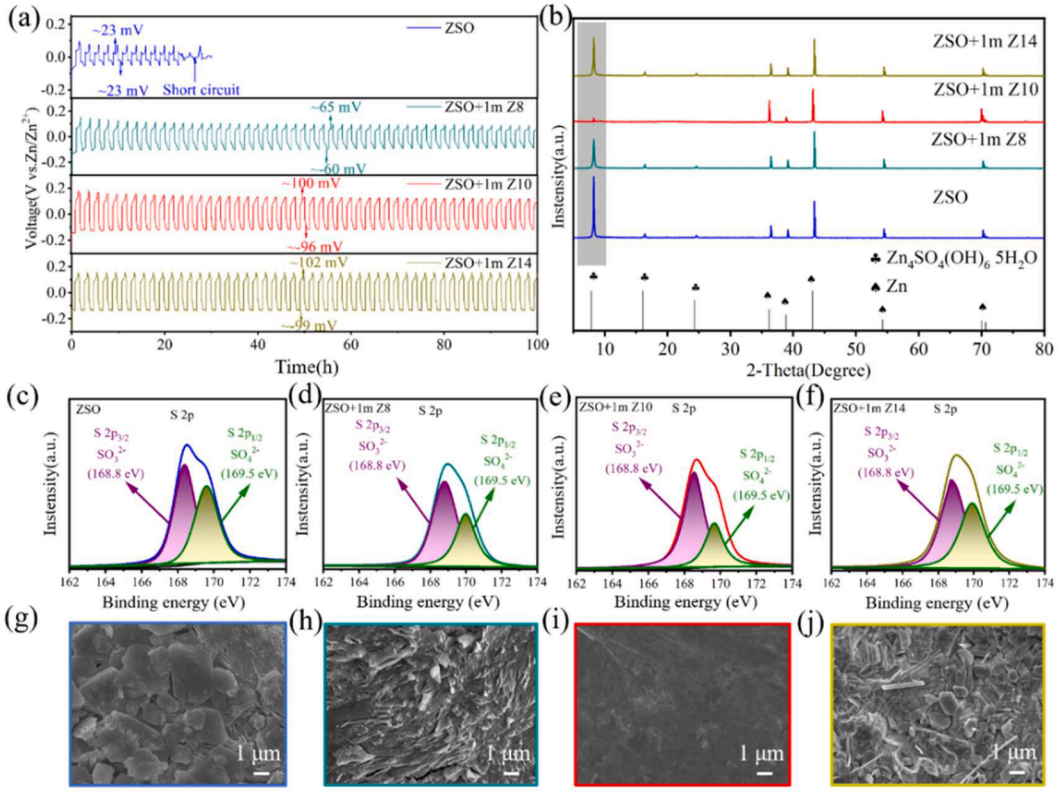

Fig. 2. (a) Galvanostatic Zn plating/stripping of Zn//Zn symmetrical batteries in different electrolytes, comparing the cycling performance achieved in the different electrolytes at a deposition capacity of 1 mAh cm^{-2} and current density of 1 mA cm^{-2}; (b) XRD patterns of Zn foils after plating/stripping cycling in the different electrolytes; S2p XPS spectra of Zn foils in ZSO electrolyte (c) and (d) ZSO+1 m Z18 electrolyte, (e) ZSO+1 m Z10 electrolyte and (f) ZSO+1 m Z14 electrolyte; SEM images of Zn foils in the ZSO electrolyte (g) and (h) ZSO+1 m Z18 electrolyte, (i) ZSO+1 m Z10 electrolyte and (j) ZSO+1 m Z14 electrolyte.

In recent years, modification of electrolytes with additives has been used to regulate the electric field distribution on the zinc electrode surface to suppress the uneven deposition of zinc and improve the cycling performance of AZIBs [16]. Surfactants are considered to have enormous potential in effectively preventing zinc dendrite formation in AZIBs due to their ability of modify both bulk and interfacial interactions. Typically, surfactants in the electrolyte can adsorb on the zinc electrode surface, thus adjusting the local current density at the electrode tip. Furthermore, the adsorption of surfactants blocks free diffusion of zinc ions at the zinc electrode surface, leading to increased nucleation sites and uniform zinc deposition [17,18]. Both cationic or anionic surfactants have been extensively studied for use as electrolyte additives in AZIBs, e.g. benzyl trimethylammonium chloride, [19] sodium dodecyl sulfate, [20] sodium dodecyl benzene sulfonate, [21] dodecyl trimethylammonium bromide, [22] tetrabutylammonium sulfonate, [23] and cetyltrimethyl ammoniumbromide [24]. Zwitterionic surfactants have large dipole moments, [25,26] which could adsorb on the electrode surface and influence ions transport in the electrolyte. However, their application as electrolyte additives and the corresponding novel mechanism has not been developed in AZIBs.

Herein, three zwitterionic surfactants, *N*-octyl-*N,N*-dimethyl-3-ammonio-1-propanesulfonate (Z8), *N*-decyl-*N,N*-dimethyl-3-ammonio-

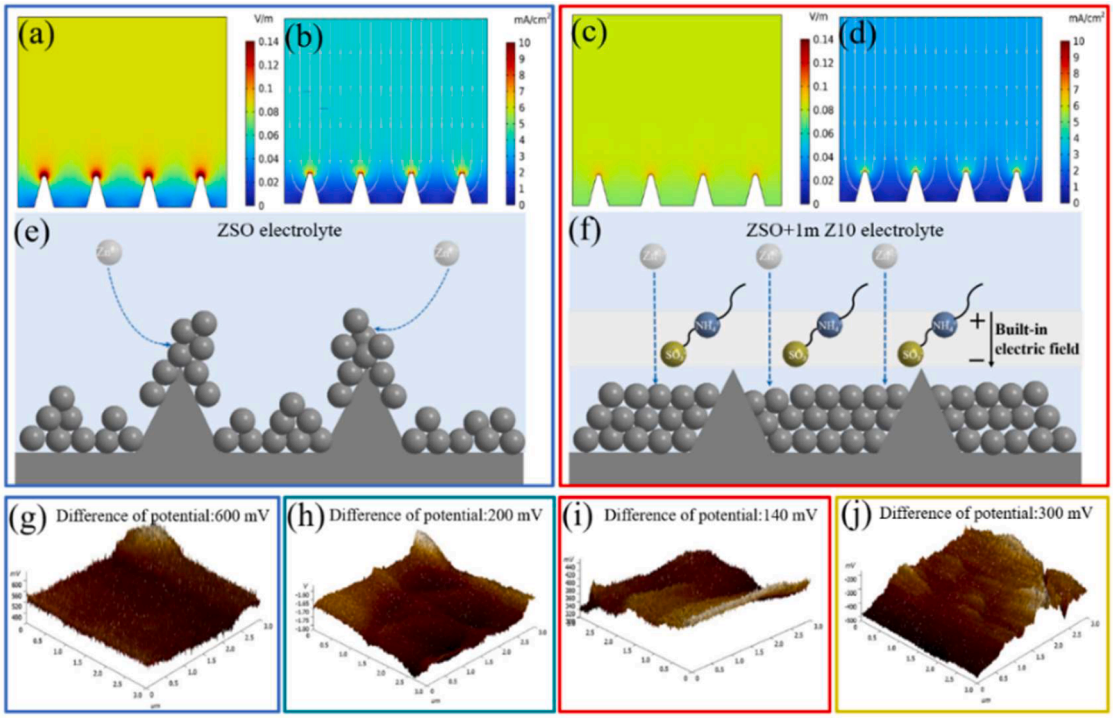

Fig. 3. Potential distribution and current density distribution at the zinc anode/electrolyte interface simulated using Simulated caculation: (a, b) ZSO electrolyte; (b, c) ZSO+1 m Z10 electrolyte; (e, f) schematics showing the deposition of zinc ions on the Zn foil; KPFM images of the ZSO electrolyte (g), and (h) ZSO+ 1 m Z8 electrolyte, (i) ZSO+1 m Z10 electrolyte and (j) ZSO+1 m Z14 electrolyte.

1-propanesulfonate (Z10) and *N*-tetradecyl-*N,N*-dimethyl-3-ammonio-1-propanesulfonate (Z14), see Fig. S1, were evaluated as electrolyte additives in AZIBs. Zwitterionic surfactants differ from other reported additives, as they have an internal molecular dipole moment that generates a built-in electric field. In the case of Z10, the lifetime of the AZIB is considerably prolonged, benefiting from the dual protection of the adsorbed layer constructed by Z10. A schematic illustration on the role of the zwitterionic surfactants in AZIBs is shown in Fig. 1.

2. Results and discussion

Initially the electrolytes were studied in Zn//Zn symmetric coin batteries assembled for galvanostatic cycling at a current density of 1 mA cm^{-2} and deposition capacity of 1 mAh cm^{-2}. The control electrolyte (termed as ZSO) comprises a $ZnSO_4$ aqueous solution (2 mol L^{-1}). 1 mmol L^{-1} of the zwitterionic surfactants, Z8, Z10 and Z14, were added to ZSO, respectively, termed as ZSO+1 m Z8, ZSO+1 m Z10 and ZSO+1 m Z14, respectively.

The performance curves of the Zn//Zn symmetrical coin batteries containing the different electrolytes over 100 charge-discharge cycles are shown in Fig. 2a. The polarization overpotential of the control battery with the ZSO electrolyte is unstable and suddenly short-circuits when cycled for 25 h. The zwitterionic surfactants adsorb at the interface between the electrolyte and the zinc anode, thereby reducing the electrochemical activity at the anode surface, leading to an increased polarization voltage. Furthermore, as the length of the alkyl chain increases in the three additives (Z8, Z10, Z14), it is possible that spatial steric hindrance and the transfer energy barrier of zinc ions also increases, resulting in an increase in polarization potential [27]. Compared to the ZSO base battery, the cycle life span of the batteries with zwitterionic surfactants are all extended beyond 100 h. XRD patterns of the Zn foils after plating/stripping cycling in the different electrolytes are shown in Fig. 2b. Characteristic peaks at 8.07°, 16.22° and 24.43° corresponding to ZHS, which could be observed on the Zn foil anode from the ZSO-based control battery. The sulfur 2p (S2p) spectrum in the XPS (Fig. 2c–f) confirms the presence of large amounts of ZHS with the signal at 169.5 eV corresponding to the SO_4^{2-} dianion, [28] consistent with the accumulation of ZHS nanosheets apparent from the SEM image of the Zn foil anode in the same battery (Fig. 2g–j). The appearance of SO_3^{2-} in the S 2s spectrum could be attributed to the indicative of decomposition of $ZnSO_4$. The digital photos of Zn foil recycled from the Zn//Zn symmetrical coin batteries are also displayed in Fig. S3a. In the photos, the non-electroactive species can be observed on the surface of Zn foil from the control battery. Part of it is the ZHS induced by water corrosion and detrimental to device stability [29,30].

The obvious difference is that the presence of the zwitterionic surfactants in the electrolyte reduces the formation of ZHS, with the characteristic peaks in the XRD pattern corresponding to ZHS either considerably reduced or, in the case of ZSO+1 m Z10 almost invisible (Fig. 2b). This is also the case at current densities of 2 mA cm^{-2} and 5 mA cm^{-2} (Fig. S4). And the S2p signals in the XPS of the Zn foils taken from the batteries containing ZSO+1 m Z8, ZSO+1 m Z10 and ZSO+1 m Z14 (Fig. 2c-f) are also reduced (olive green area). The SEM images (Fig. 2h–j) show that different surfactants lead to different shapes of ZHS on the surface of Zn foil and the accumulation state is also different. Many ZHS nanosheets have accumulated on the surface of cycled Zn foils immersed in the electrolytes containing Z8 and Z14, whereas the surface of cycled Zn foil based on Z10 is smooth.

Additionally, as shown in Fig. S5, the adsorption energies of Z10 and water on the zinc anode surface were calculated using DFT. It was demonstrated that Z10 preferentially reaches the interface between the electrolyte and the zinc anode and forms a molecular adsorption layer due to the lower adsorption energy. Electrochemical impedance spectroscopy (EIS) and contact angle tests were performed Zn//Zn symmetric cells with different electrolytes (Figs. S6 and S7), which also showed that zwitterionic surfactants molecules adsorbed on the surface of zinc anode [31]. Furthermore, XPS and FTIR were utilized to verify that the zwitterionic surfactants interact with the zinc anode surface through sulfonate groups [32]. For detailed discussion, refer to the diagram in the supporting information (Figs. S8 and S9). Undoubtedly, the

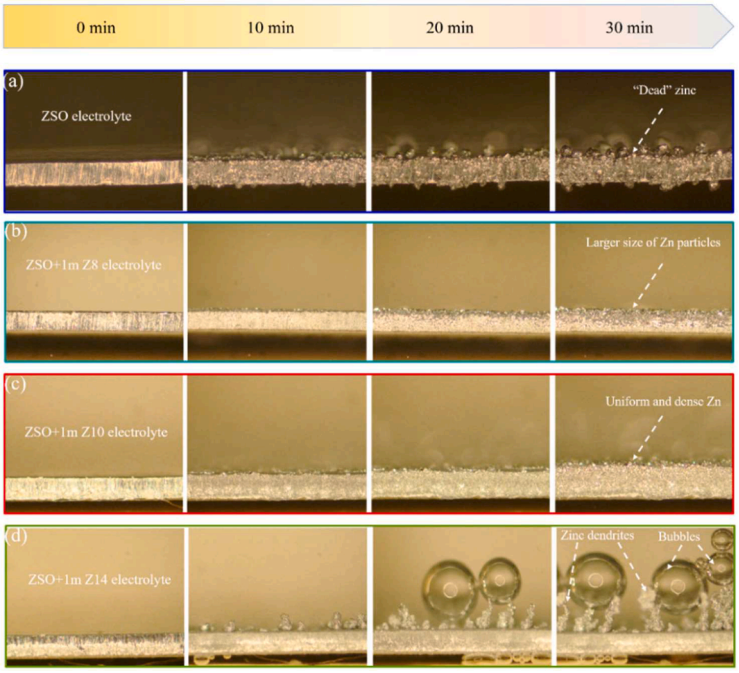

Fig. 4. In situ optical microscopy showing Zn deposition on Zn foils in the different electrolytes at a current density of 4 mA cm^{-2}: (a) ZSO electrolyte; (b) ZSO+1 m Z8 electrolyte; (c) ZSO+1 m Z10 electrolyte; (d) ZSO+1 m Z14 electrolyte.

adsorption state of zwitterionic surfactants at the electrolyte and zinc anode interface significantly affects the kinetic process of zinc ion transport. Therefore, the contact angles between the electrolyte droplets containing different surfactants and the surface of the zinc anode were measured, and the corresponding critical micelle concentration (CMC) values were also obtained. (Detailed discussion refers to Figs. S10–S13) It can be deduced that the adsorption of Z8 at the zinc anode surface is far from saturation, forming a loose multi-vacancy monolayer and increasing the risk of dendrite growth and water corrosion on the condition of 1 mmol L^{-1}. And Z14 is prone to form micelles due to supersaturated adsorption. Unfortunately, these micelles are harmful for the zinc ions transfer and disturbed the dynamic process of zinc plating/stripping. On the contrary, Z10 only forms a nearly saturated monomolecular adsorption layer at this concentration. Notably, the zwitterionic surfactants can form a dipole layer at the interface between the electrolyte and the zinc anode, resulting in a built-in electric field, which also influences the transfer of zinc ions and deposition processes (see below).

According to the measured physical parameters of different electrolytes, the electric field and current density distribution on the surface zinc anode in different electrolytes are obtained by simulated caculation simulation. As shown in Fig. 3a and b, in the battery without surfactants, the electric field distribution and current distribution on the surface of the zinc anode are non-uniform, and the "tip effect" on the crystalline surface of the zinc anode is significant, shown as red dots. The KPFM image confirms this observation (Fig. 3g), with an undulating potential distribution on the Zn foil surface after cycling with bare ZSO. The zinc ions in the electrolyte are deposited by the strong electric field on the surface of the Zn foil, gradually accumulating to form large dendrites (shown in Fig. 3e). The partial accumulation of an unevenly-deposited zinc layer presumably increases the electrode thickness, which in turn increases the risk of piercing the separator, eventually leading to short circuiting [33,34]. With the addition of 1 m Z8, 1 m Z10 and 1 m Z14, the potential difference on the Zn foil surface decreases (Figs. 3h–j and S14). Moreover, the uniform distribution of the electric field and current on the zinc anode surface is significantly improved in the presence of 1 m Z10 (Fig. 3c, d and i).

Besides XPS and FTIR, DFT calculations also indicates that the zwitterionic surfactants absorb on the surface of zinc anode via the sulfonate group, and the hydrophobic chains is oriented toward the outer Helmholtz plane (Fig. S17) [35–37]. Owing to the dipole nature of the zwitterionic surfactants, a uniform built-in electric field forms at the interface between the electrolyte and the zinc anode, with the electric field directed towards the zinc anode. Consequently, the "tip effect" on the zinc anode surface is significantly reduced, and the dendrite growth is greatly suppressed. Additionally, the presence of the built-in electric field modulates the deposition rate of zinc ions, promoting a uniform deposition, as evident from in situ optical microscopy studies. However, not all three zwitterionic surfactants can facilitate uniform zinc deposition. This is because the length of the hydrophobic alkyl chain affects the self-assembly conformation of the zwitterionic surfactant on the zinc anode surface, thereby influencing the built-in electric field and inhibitory effect on the "tip effect". Assuming all three types of molecules are in a monolayer of saturated adsorption, then the strength of the built-in electric field depends on the adsorption angle between the molecules and the zinc negative electrode surface.(Fig. S17) The greater the angle, the stronger the corresponding electric field. Therefore, it can be concluded that compared to Z8 and Z14, Z10 has a stronger embedded electric field (Figs. 3c and S14). Furthermore, considering that Z8 cannot form saturated adsorption and Z14 forms micelles due to oversaturated adsorption (as the results of CMC), it means that only Z10 can effectively form an appropriate molecular adsorption layer and a built-in electric field, thus providing the best suppression effect on the "tip effect" and results in a largest zinc ion transfer (0.81) and exchange current densities (3.92 mA cm^{-2}), see Figs. S16–S18 for further details.

In situ optical microscopy was used to monitor the changes to the Zn foil in the different electrolytes during a 30 min deposition process (Fig. 4). At the initial state, a bright galvanized layer with metallic luster is observed on the surface of the Zn foil in the ZSO electrolyte. As the deposition time increased to 30 min, prominent bulges, and a mass of "dead zinc" appeared on the surface and sides of the Zn foil after 30 min plating, as observed elsewhere. Severe side reactions on the anode surface and the occurrence of "dead zinc" caused by dendrites will rapidly shorten the lifespan of the control battery [38]. After adding 1 m Z8 to the ZSO electrolyte, the phenomenon of "dead zinc" was somewhat alleviated. However, due to the non-dense molecular adsorption layer of

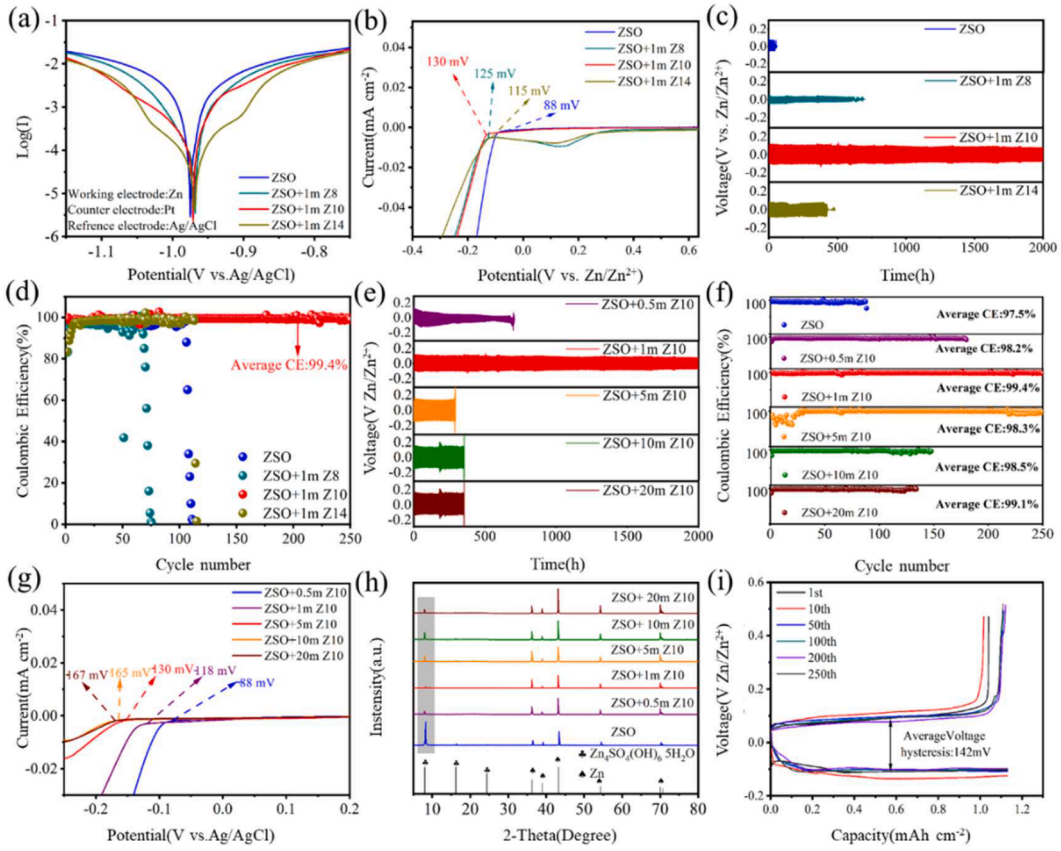

Fig. 5. (a) Tafel and (b) LSV curves (HER) of the different electrolytes; (c) galvanostatic Zn plating/stripping of long-term cyclic stability of Zn//Zn symmetrical batteries with different electrolytes at a current density of 1 mA cm^{-2} and the area capacity of 1 mAh cm^{-2}; (d) CE measurements of Zn//Cu batteries using the different electrolytes; The ZSO electrolyte with different concentrations of Z10 (0.5, 1, 5, 10 and 20 mmol L^{-1}, termed 0.5 m Z10, 1 m Z10, 5 m Z10, 10 m Z10 and 20 m Z10, respectively): (e) galvanostatic Zn plating/stripping of long-term cyclic stability of Zn//Zn symmetrical batteries containing the different electrolytes at a current density of 1 mA cm^{-2} with area capacity of 1 mAh cm^{-2}, (f) CE measurements of Zn//Ti half batteries containing the different electrolytes; (g) LSV curves (HER), and (h) comparison of XRD patterns of Zn foils after 50 cycles using the different electrolytes; (i) voltage profiles of Zn plating/stripping of Zn//Ti half batteries in the ZSO+1 m Z10 electrolyte.

Z8, the galvanized layer remained uneven and loose, and large particles were observed on the surface and sides of the Zn foil [39,40]. This indicates that Z8 does not provide a sufficient hydrophobic effect, and water molecules can still come into contact with the zinc anode surface to cause corrosion. The Zn foil obtained in the electrolyte doped with 1 m Z14 formed dendrites and micelles on the surface of Zn foil. The CMC value of Z14 is $\leq$ 0.5 mmol L^{-1}, hence Z14 forms micelles on the zinc anode surface at the additive concentration of 1 mmol L^{-1}, as observed by in situ optical microscopy. In contrast, the CMC of Z8 and Z10 is ~5 mmol L^{-1} and ~2.5 mmol L^{-1}, respectively, and therefore micelles do not form. The micelles at the electrolyte and anode interface hinder the stable transfer of zinc ions and the plating/stripping of zinc [17,41]. After running for 30 min, the battery based on 1 m Z10 battery does not exhibit any "dead zinc" areas, but instead of a uniformly dense zinc-plated layer. This is due to during zinc deposition process, the additive molecules undergo directional adsorption behavior at the interface of electrolyte/zinc anode through the hydrophilic sulfonate group. The hydrophobic alkyl long chains of the additive molecules in the adsorption layer extend into the electrolyte to form a hydrophobic layer, preventing the movement and contact of the water molecules inside the electrolyte on the zinc anode surface, which inhibits the corrosion of zinc from H_2O molecules.

The corrosion current and potential on the zinc anode surface under different electrolytes were obtained from Tafel curves (Figs. 5a and S19). Compared with the corrosion current of the battery based on the ZSO electrolyte (0.96 mA cm^{-2}), the addition of zwitterionic surfactants reduced the corrosion current of the battery. Among them, the lowest corrosion current at 0.38 mA cm^{-2} was obtained for the ZSO+1 m Z10 based battery. The HER curves also showed the hydrogen evolution potential is highest in the ZSO electrolyte containing 1 m Z10 (Fig. 5b). In addition, we prepared Zn//Zn symmetric coin batteries with different electrolytes, and evaluated with plating/striping cycles under the conditions of a current density of 1 mA cm^{-2} and a deposition capacity of 1 mAh cm^{-2}. As shown in Fig. 5c, the control cell cycled only about 100 h, while the Z14-based battery experienced a sudden voltage drop after 420 h of cycling, indicating battery failure. Similarly, the Z8-based battery also exhibited a similar voltage drop after stable cycling for 650 h. In contrast, the battery using ZSO+1 m Z10 electrolyte showed minimal potential fluctuations that can be neglected, and ultimately achieved stable cycling for over 2000 h.

To further identify Z10 as the optimal additive molecule, 250 cycles were conducted on the Zn//Cu half-battery to evaluate the Coulombic efficiency (CE) of the zinc plating/stripping process. From Fig. 5d, it can be observed that among several batteries, only the battery containing 1 m Z10 electrolyte could maintain stable cycling, with a CE as high as 99.4%. These results indicate that among the three additives, Z10 possesses the optimal molecular configuration, capable of forming a suitable hydrophobic molecular adsorption layer and a build-in electric field. It synergistically acts on the zinc plating/striping process, preventing water corrosion of zinc anode while promoting the transfer and unform zinc deposition. To investigate the optimal additive concentration for Z10, the cycling performances of half-battery at different additive concentrations were also measured. Only when the additive concentration was 1 mmol L^{-1}, the Z10-based battery exhibited stable

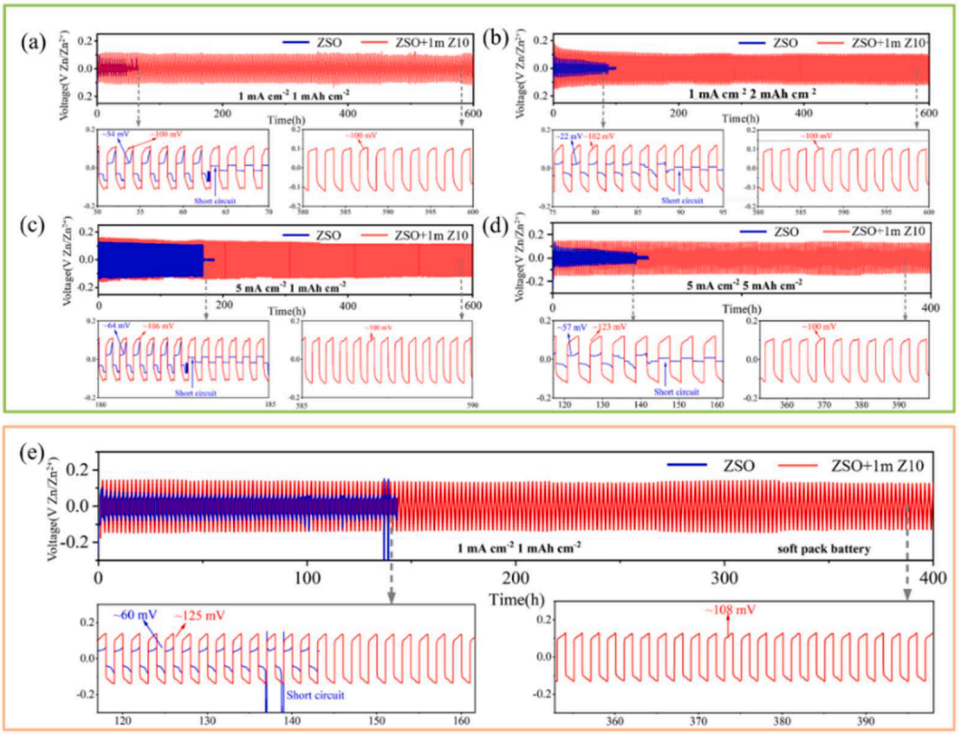

Fig. 6. (a-d) Comparison of galvanostatic Zn plating/stripping and long-term cyclic stability of Zn//Zn symmetrical coin batteries based on ZSO and ZSO+1 m Z10 electrolytes at different current density and area capacity; (e) comparison of galvanostatic Zn plating/stripping in Zn//Zn soft pack batteries using the two electrolytes.

and long-lasting cycling for over 2000 h (Fig. 5e) and achieved a Coulombic efficiency (CE) of over 99.4 % (Fig. 5f). Moreover, the corrosion potential of the zinc foil after cycling (Fig. 5g) indicated that a suitable corrosion potential was achieved at the concentration of 1 mmol L^{-1}. And the XRD spectrum (Fig. 5h) at this concentration showed negligible ZHS peaks, indicating the suppression of side reactions and their byproduct ZHS. When the concentration of Z10 is relatively low, i.e., $<$ 1 mmol L^{-1}, a saturated adsorption layer cannot form on the zinc anode surface, resulting in significant gaps between molecules and ineffective prevention of water erosion on the anode, thus leading to the formation of ZHS. Simultaneously, under this condition, the built-in electric field generated by Z10 is insufficient to accelerate the transport of zinc ions, which is detrimental to improving the coulombic efficiency of the battery. As the concentration of Z10 increases to 5 mmol L^{-1} or even higher, the adsorption of Z10 on the zinc anode surface reached saturation or over-saturation. Consequently, Z10 molecules are

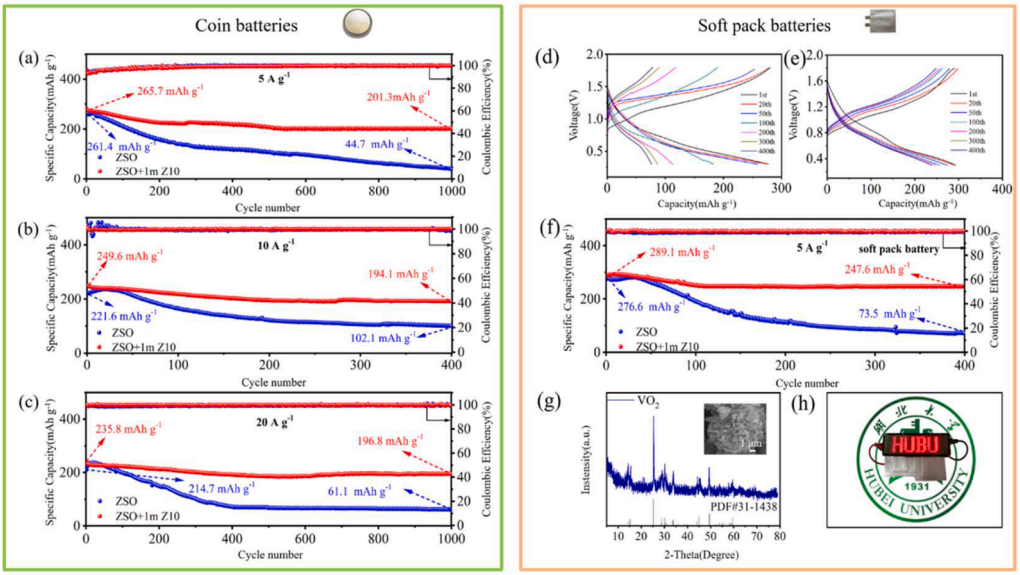

Fig. 7. (a-c) Comparison of the cycle stability performance of coin batteries for Zn//VO_2 using ZSO and ZSO+1 m Z10 electrolytes at different current densities; (d-e) charge–discharge curves of soft pack batteries for Zn//VO_2 with different cycle numbers in the two electrolytes; (f) cycle stability performance of soft pack batteries for Zn//VO_2 in two electrolytes; (g) VO_2 XRD patterns and SEM images of the powder (inset); (h) lighting test for Zn//VO_2 soft-pack batteries with ZSO+1 m Z10 electrolytes.

prone to form micelles or vesicles at the electrolyte-electrode interface, hindering the transport and deposition of zinc ions and increasing the overpotential (Fig. S22) [19]. Simultaneously, the micelles also destabilize the interface, leading to a significant decrease in the cycling stability of the device (Fig. 5f). Ultimately, when the optimal concentration is 1 mmol L^{-1}, the battery exhibited a longer cycling life, lower overpotential (142 mV) as shown in Fig. 5i, and a higher zinc ion transfer number (Figs. S22 and S23).

The service life under different current densities is an important evaluation criterion for the commercialization of AZIBs. Therefore, we investigated the long-term cycling performance of Zn//Zn symmetrical coin batteries containing ZSO and ZSO+1 m Z10 electrolytes at different current densities and areal capacities (Fig. 6a–d). Under both high and low current density and areal capacity conditions, batteries assembled with bare ZSO electrolyte show a short circuit after approximately 100 h. However, after adding 1 m Z10, the battery can stably cycle for up to 400–600 h under various conditions, while maintaining a stable polarization overpotential. In addition, we compared the CE and hysteresis voltage of Zn//Cu batteries based on ZSO and ZSO+1 M Z10 under conditions of 1 mAh cm^{-2} and 2 mAh cm^{-2} (Fig. S26). The Zn//Cu battery with ZSO+1 m Z10 electrolyte exhibited extremely stable and over 300 cycles, with a CE of 99.2 %. This indicated a highly reversible zinc plating/stripping process. Zn//Zn soft pack symmetric batteries were also assembled and cycled under the same conditions, i.e.1 mA cm^{-2} and 1 mA cm^{-2} (Fig. 6e). Similar to coin batteries, soft pack batteries using ZSO+1 m Z10 electrolyte exhibited stable polarization over 400 cycles. However, ZSO-based electrolyte batteries experience severe swelling (Fig. S27) due to hydrogen evolution reaction on the surface of the zinc anode, and eventually fail after 137 h.

Vanadium oxide materials, especially VO_2, as cathode materials have attracted increasing interest over the last few years, due to their variety of accessible oxidation states, high theoretical capacities (generally >300 mAh g^{-1}), unique tunnel transport pathway and low cost [42]. The VO_2 used as cathode material of AZIBs in this work was prepared according to our previous method, [19] which involves modification by ascorbic acid to enhance the structural stability and electrochemical performance of the VO_2 cathode material (Fig. 7 g). The full coin and soft pack batteries with VO_2 as the cathode material were encapsulated (Zn//VO_2 full battery) and studied. From Fig. 7a, after 1000 cycles at 5 A g^{-1}, the ZSO-based battery deteriorated rapidly, and the discharge specific capacity was only 44.7 mAh g^{-1} while the initial value was 261.4 mAh g^{-1}. However, with the ZSO+1 m Z10 electrolyte, the battery maintains a high discharge specific capacity of 201.3 mAh g^{-1} (cf. the initial specific capacity of 265.7 mAh g^{-1}) and the CE remains at 99 %. Superior reversibility in the CV curves and higher reversibility of voltage in the charge/discharge curves at different cycle times are also observed, see Figs. S26 and S27, respectively. Increasing the current density to 10 A g^{-1} (Figs. 7b and S28), the Zn//VO_2 battery with the ZSO+1 m Z10 electrolyte has a higher discharge specific capacity of 194.1 mAh g^{-1} compared to the initial value of 249.9 mAh g^{-1} after 400 cycles. Under the same conditions, the ZSO electrolyte-based battery has a discharge specific capacity of 61.1 mAh g^{-1} (cf. initially 214.7 mAh g^{-1}). A similar phenomenon is observed at the higher current density cycle of 20 A g^{-1} (Figs. 7c, and S29). The Zn//VO_2 full battery with 1 m Z10 exhibited a high capacity of 196.8 mAh g^{-1} after 1000 cycles, the capacity retained is nearly 100 %, which is much larger than that control battery. In contrast, batteries with the ZSO electrolyte have poor capacity retention after long-term cycling regardless of the current density. There is also a notable difference in the cycling performance of Zn//VO_2 flexible soft pack batteries between the electrolytes at a current density of 5 A g^{-1} (Fig. 7d–f). After 400 cycles, the initial discharge capacity of the Zn//VO_2 flexible pack battery with the ZSO+1 m Z10 electrolyte is 247.6 mAh g^{-1}, whereas with the ZSO electrolyte the Zn//VO_2 flexible pack battery decays to only 73.5 mA h g^{-1}, and shows severe bulging preventing operation. To further demonstrate the practicality of the 1 m Z10 based electrolyte, two Zn//VO_2 soft pack batteries were successfully used to light a LED, as shown in Fig. 7h.

3. Conclusions

To enhance the long-term stability of zinc anodes in AZIBs, three zwitterionic surfactants (Z8, Z10 and Z14) were employed as electrolyte additives. The zwitterionic surfactants can self-assemble at the interface of electrolyte and zinc anode, forming a hydrophobic effect because of their long alkyl chains. The hydrophobic barrier provided by Z10 prevents contact of water in the electrolyte with the surface of zinc anode, thus suppressing the generation of ZHS and prolonging the battery cycle life. The length of the alkyl chain is crucial. If it is too short, as in Z8, an ideal dense and flat monolayer cannot be obtained on the zinc anode, and there is still a risk of water corrosion. If it is too long, as in Z14, the surfactants are prone to form micelles in the electrolyte, leading to the formation of many dendrites on the surface of the zinc anode. In both cases, the zinc anode has a low lifespan. However, by using Z10, a dense galvanized coating without "dead zinc" can be achieved, resulting in a zinc anode with a long cycle life. Compared with other reported cationic and anionic surfactants, the zwitterionic surfactants used here provide a build-in electric field. The strength of the electric field is influenced by the alkyl chain length on the surfactants, with the alkyl chain length of Z10 being optimal for forming a uniformly distributed electric field on the zinc electrode surface. Therefore, Z10 surfactant inhibits the "tip effect" on the zinc anode surface, promotes the rapid transfer of zinc ions, enables uniform zinc deposition, and significantly extends the lifespan of the zinc anode. At the optimal Z10 concentration of 1 mmol L^{-1}, encapsulated coin and soft batteries employing VO_2 as a cathode material were fabricated, and a high reversibility approach and a near-quantitative CE obtained. These findings provide a new insight for developing novel surfactants for long-life zinc anode batteries.

Credit author statement

Li Tao, Hao Wang and Mohammad Khaja Nazerruddinc conceived the research project. Rong Yang, Haonan Zhang and Kailin Guan fabricated and tested the zinc ions batteries. Longyang Wang and Houzhao Wan performed the KPFM tests. Zhongxin Guo carried out the theoretical calculation. Jun Zhang and Hanbin Wang recorded the SEM and analyzed the results of the electrochemical tests. Paul J. Dyson supervised different parts of the work and polished the manuscript. Rong Yang and Li Tao wrote the paper. And all authors contributed to the data analysis and commented on the manuscript.

Declaration of Competing Interest

There are no conflicts of interest to declare.

Data availability

Data are provided as SI.

Acknowledgements

The authors are grateful for financial support from the National Natural Science Foundation of China (No. 52272198, 52171203), the Natural Science Foundation of Jiangsu Province (Grants No. BK20211516), the National Key Research and Development Program of China (Grant No. 2021YFB2400400), and the Fundamental Research Funds for the Central Universities (2242023K5001).

Supplementary materials

Supplementary material associated with this article can be found, in the online version, at doi:10.1016/j.ensm.2023.102981.

References

[1] P. Albertus, S. Babinec, S. Litzelman, Nat. Energy 3 (2018) 16–21.
[2] L. Mai, M. Yan, Y. Zhao, Nature 546 (2017) 469–470.
[3] A. Manthiram, X. Yu, S. Wang, Nat. Rev. Mater. 2 (2017) 16103.
[4] A. Yoshino, Angew. Chem. Int. Ed. 51 (2012) 5798–5800.
[5] X. Zeng, M. Li, D. Abd El-Hady, W. Alshitari, A.S. Al-Bogami, J. Lu, K. Amine, Adv. Energy Mater. 9 (2019), 1900161.
[6] Y. Lu, X. Rong, Y.-S. Hu, L. Chen, H. Li, Energy Storage Mater. 23 (2019) 144–153.
[7] H. Yang, Y. Qiao, Z. Chang, H. Deng, X. Zhu, R. Zhu, Z. Xiong, P. He, H. Zhou, Adv. Mater. 33 (2021), 2102415.
[8] J. Zheng, Z. Cao, F. Ming, H. Liang, Z. Qi, W. Liu, C. Xia, C. Chen, L. Cavallo, Z. Wang, H.N. Alshareef, ACS Energy Lett. 7 (2022) 197–203.
[9] J. Zhou, M. Xie, F. Wu, Y. Mei, Y. Hao, L. Li, R. Chen, Adv. Mater. 34 (2022), 2106897.
[10] H. Yang, T. Zhang, D. Chen, Y. Tan, W. Zhou, L. Li, W. Li, G. Li, W. Han, H.J. Fan, D. Chao, Adv. Mater. (2023), 2300053 n/a.
[11] Z. Yang, B. Wang, Y. Chen, W. Zhou, H. Li, R. Zhao, X. Li, T. Zhang, F. Bu, Z. Zhao, W. Li, D. Chao, D. Zhao, Natl. Sci. Rev. 10 (2023) nwac268.
[12] Y. Qin, P. Liu, Q. Zhang, Q. Wang, D. Sun, Y. Tang, Y. Ren, H. Wang, Small 16 (2020), 2003106.
[13] R. Zhao, X. Dong, P. Liang, H. Li, T. Zhang, W. Zhou, B. Wang, Z. Yang, X. Wang, L. Wang, Z. Sun, F. Bu, Z. Zhao, W. Li, D. Zhao, D. Chao, Adv. Mater. 35 (2023), 2209288.
[14] W. Zhou, M. Song, P. Liang, X. Li, X. Liu, H. Li, T. Zhang, B. Wang, R. Zhao, Z. Zhao, W. Li, D. Zhao, D. Chao, J. Am. Chem. Soc. 145 (2023) 10880–10889.
[15] W. Du, E.H. Ang, Y. Yang, Y. Zhang, M. Ye, C.C. Li, Energy Environ. Sci. 13 (2020) 3330–3360.
[16] Q. Zhang, J. Luan, Y. Tang, X. Ji, H. Wang, Angew. Chem. Int. Ed. 59 (2020) 13180–13191.
[17] R. Atkin, V.S.J. Craig, E.J. Wanless, S. Biggs, Adv. Colloid Interface Sci. 103 (2003) 219–304.
[18] F. Seidi, D. Crespy, Chem. Commun. 56 (2020) 11931–11940.
[19] K. Guan, L. Tao, R. Yang, H. Zhang, N. Wang, H. Wan, J. Cui, J. Zhang, H. Wang, H. Wang, Adv. Energy Mater. 12 (2022), 2103557.
[20] Z. Hou, X. Zhang, X. Li, Y. Zhu, J. Liang, Y. Qian, J. Mater. Chem. A 5 (2017) 730–738.
[21] J. Hao, J. Long, B. Li, X. Li, S. Zhang, F. Yang, X. Zeng, Z. Yang, W.K. Pang, Z. Guo, Adv. Funct. Mater. 29 (2019), 1903605.
[22] K. Liu, P. He, H. Bai, J. Chen, F. Dong, S. Wang, M. He, S. Yuan, Mater. Chem. Phys. 199 (2017) 73–78.
[23] A. Bayaguud, X. Luo, Y. Fu, C. Zhu, ACS Energy Letters 5 (2020) 3012–3020.
[24] K. Sai Jyotheender, M.K. Punith Kumar, C. Srivastava, Influence of surfactant polarity on the evolution of micro-texture, Surf. Coat. Technol. 423 (2021), 127594.
[25] Z. Chen, W.Q. Lu, J. Liu, K. Amine 51 (2006) 3322–3326.
[26] R. Rondla, J.C.Y. Lin, C.T. Yang, I.J.B. Lin, Langmuir 29 (2013) 11779–11785.
[27] Y. Zhu, M.L. Free, R. Woollam, W. Durnie, Prog. Mater Sci. 90 (2017) 159–223.
[28] C. Huang, X. Zhao, S. Liu, Y. Hao, Q. Tang, A. Hu, Z. Liu, X. Chen, Adv. Mater. 33 (2021), 2100445.
[29] Z. Hou, Y. Gao, H. Tan, B. Zhang, R Nat. Commun. 12 (2021) 3083.
[30] L.E. Blanc, D. Kundu, L.F. Nazar, Scientific challenges for the implementation of Zn-ion batteries, Joule 4 (2020) 771–799.
[31] H. Dai, X. Gu, J. Dong, C. Wang, C. Lai, S. Sun, Nat. Commun. 11 (2020) 643.
[32] Y. Lv, M. Zhao, Y. Du, Y. Kang, Y. Xiao, S. Chen, Energy Environ. Sci. 15 (2022) 4748–4760.
[33] C. Li, Z. Sun, T. Yang, L. Yu, N. Wei, Z. Tian, J. Cai, J. Lv, Y. Shao, M.H. Rümmeli, J. Sun, Z. Liu, Adv. Mater. 32 (2020), 2003425.
[34] P. Xue, C. Guo, L. Li, H. Li, D. Luo, L. Tan, Z. Chen, Adv. Mater. 34 (2022), 2110047.
[35] S. Xu, M. Chen, E. Cholewa, G. Szymanski, J. Lipkowski, Langmuir 23 (2007) 6937–6946.
[36] I. Phiri, C.Y. Bon, M. Mwemezi, L. Hamenu, A. Madzvamuse, J.H. Park, K.S. Lee, J. M. Ko, Y. Lu, Mater. Chem. Phys. 243 (2020), 122577.
[37] M. Luo, X. Gan, X. Zhao, L. Huang, H. Zhu, X. Yan, K. Shi, J. Alloys Compd. 918 (2022), 165790.
[38] J. Hao, X. Li, X. Zeng, D. Li, J. Mao, Z. Guo, Energy Environ. Sci. 13 (2020) 3917–3949.
[39] R. Qin, Y. Wang, M. Zhang, Y. Wang, S. Ding, A. Song, H. Yi, L. Yang, Y. Song, Y. Cui, J. Liu, Z. Wang, S. Li, Q. Zhao, F. Pan, Nano Energy 80 (2021), 105478.
[40] X. Gao, Y.-N. Zhou, D. Han, J. Zhou, D. Zhou, W. Tang, J.B. Goodenough, Joule 4 (2020) 1864–1879.
[41] Z. Chang, X. Chen, Y. Peng, Miner. Eng. 121 (2018) 66–76.
[42] K. Guan, K. Duan, G. Yang, L. Tao, H. Zhang, H. Wan, R. Yang, J. Zhang, H. Wang, H. Wang, Mater. Today Adv. 14 (2022), 100230.